



Deposited via The University of Leeds.

White Rose Research Online URL for this paper:

<https://eprints.whiterose.ac.uk/id/eprint/80239/>

Version: Accepted Version

Article:

Moazen, M, Mak, JH, Etchels, LW et al. (2013) The effect of fracture stability on the performance of locking plate fixation in periprosthetic femoral fractures. *Journal of Arthroplasty*, 28 (9). 1589 - 1595. ISSN: 0883-5403

<https://doi.org/10.1016/j.arth.2013.03.022>

Reuse

Items deposited in White Rose Research Online are protected by copyright, with all rights reserved unless indicated otherwise. They may be downloaded and/or printed for private study, or other acts as permitted by national copyright laws. The publisher or other rights holders may allow further reproduction and re-use of the full text version. This is indicated by the licence information on the White Rose Research Online record for the item.

Takedown

If you consider content in White Rose Research Online to be in breach of UK law, please notify us by emailing eprints@whiterose.ac.uk including the URL of the record and the reason for the withdrawal request.

1 **The effect of fracture stability on the performance of locking plate fixation**
2 **in periprosthetic femoral fractures**

3
4 **Mehran Moazen, PhD^{1,2}**
5 **Jonathan H. Mak, MEng¹**
6 **Lee W. Etchels, MEng¹**
7 **Zhongmin Jin, PhD^{1,3}**
8 **Ruth K. Wilcox, PhD¹**
9 **Alison C. Jones, PhD¹**

10 **Eleftherios Tsiridis, MD, MSc, PhD, FRCS^{4,6}**

- 11
12
13
14 1. Institute of Medical and Biological Engineering,
15 School of Mechanical Engineering,
16 University of Leeds,
17 Leeds, LS2 9JT, UK
18
19 2. Medical and Biological Engineering,
20 School of Engineering,
21 University of Hull,
22 Hull, HU6 7RX, UK
23
24 3. Institute of Advanced Manufacturing Technology,
25 School of Mechanical Engineering,
26 Xi'an Jiaotong University,
27 Xi'an, 710049, P.R. of China
28
29 4. Academic Department of Orthopaedic and Trauma,
30 University of Leeds,
31 Leeds, LS2 9JT, UK
32
33 5. Department of Surgery and Cancer, Division of Surgery,
34 Imperial College London,
35 London, W12 0HS, UK
36
37 6. Academic Orthopaedics and Trauma Unit,
38 Aristotle University Medical School,
39 University Campus 54 124, Thessaloniki, Greece
40

41
42 **Corresponding author:**

43 Mehran Moazen, PhD
44 Medical and Biological Engineering,
45 School of Engineering,
46 University of Hull, Hull, HU6 7RX
47 Tel: +44 (0) 1482 466760
48 Fax: +44 (0) 1482 466664
49 Email: Mehran_Moazen@yahoo.com; M.Moazen@hull.ac.uk
50

51 **The effect of fracture stability on the performance of locking plate fixation**
52 **in periprosthetic femoral fractures**

53

54

55 **Abstract**

56 Periprosthetic femoral fracture (PFF) fixation failures are still occurring. The effect of fracture
57 stability and loading on PFF fixation has not been investigated and this is crucial for optimum
58 management of PFF. Models of stable and unstable PFFs were developed and used to
59 quantify the effect of fracture stability and loading in a single locking plate fixation. Stress on
60 the plate was higher in the unstable compared to the stable fixation. In the case of unstable
61 fractures, it is possible for a single locking plate fixation to provide the required mechanical
62 environment for callus formation without significant risk of plate fracture, provided partial
63 weight bearing is followed. In cases where partial weight bearing is unlikely, additional
64 biological fixation could be considered.

65

66

67

68 **Keywords:** fracture movement, weight bearing, strain, stiffness, finite element method

69 **Running title:** Biomechanics of periprosthetic femoral fracture fixation

70

71

72

73

74

75

76 **1. Introduction**

77 Periprosthetic femoral fractures (PFF) can occur following primary total hip arthroplasty
78 (THR) [1-6]. The management of these fractures is becoming increasingly important due to
79 rise in number of THRs [4], but is challenging due to the presence of the underlying
80 prosthesis. Over recent years there have been a number of fixation failures reported in the
81 literature including instances of fixation plate fracture [3,5,7]. Interestingly, it appears that
82 most Vancouver B1 [1] PFF fixation failures were initially transverse fractures [5],
83 considering that if no gap were present at the fracture site postoperatively, these would have
84 been stable fractures with good bone quality. Nevertheless, overloading of the fixation plates
85 can cause local stress concentrations [5] which result in progressive damage over multiple
86 loading cycles and can cause plate fracture. Analysis of the construct geometry and loading
87 conditions which create these peaks of stress is therefore of interest.

88 Several authors have compared the application of various plates with different
89 configurations of locking and non-locking screws and cables to find the optimum fixation for
90 PFF [8-11]. However, these studies are commonly carried out on a particular fracture
91 configuration and loading with either stainless steel (SS) or titanium (Ti) plate. The success of
92 any one of these fixation constructs also depends on the configuration of the bone fracture and
93 its stability once reduced. For example simple, transverse (stable) fracture may allow for load
94 transfer at the fracture site, where a severely comminuted (unstable) fracture may not.

95 A number of factors including fracture stability, loading and material properties of the
96 fixation device will play a role in the stiffness of the construct, level of fracture movement
97 and subsequent healing mode of the fracture [12-15]. The effect of fracture stability and
98 loading on either SS or Ti plates in PFF fixation does not appear to have been investigated
99 and this is fundamental for optimum management of PFF.

100 Experimental in vitro models have been commonly used to test different fixation
101 methods for PFF in terms of stiffness, fracture movement or surface strain [8-11].
102 Computational models based on the finite element (FE) method allow the full pattern of strain
103 and stress distribution to be assessed, as well as providing the flexibility to test a wide range
104 of cases [16-19]. However, the computational model validity needs to be demonstrated [20].
105 Comparison with experimental in vitro data may be used to provide confidence in the model
106 predictions, but, as yet, such corroborated FE models of PFF fixation are surprisingly rare
107 [18].

108 In this study a FE model of the fixation of a Vancouver type B1 PFF within a stable
109 stem with good bone quality [1] was developed. The predictions of the model were first
110 compared with experimental tests to corroborate mechanical behaviour, with particular
111 emphasis on the fixation plate. This model was then used to address aims of this study: (1) to
112 quantify the effect of fracture stability on the performance of a locking plate fixation (2) to
113 compare the performance of SS versus Ti plate fixations in stable and unstable fracture under
114 two weight bearing conditions. The overall hypothesis of this study is that fracture stability
115 can considerably affect the performance of both SS and Ti locking plates in PFF fixation.

116

117 **2. Materials and Methods**

118 In the first step, FE models of stable (with no gap at the fracture site) and unstable (with a
119 10mm gap at the fracture site) periprosthetic fracture cases were developed to match
120 corresponding instrumented experimental models that were mechanically tested in the
121 laboratory. The stiffness, surface strain and fracture movement were compared. Following
122 this, in the second step, the FE models were altered to compare the performance of the SS
123 versus Ti plate in the stable and unstable PFF fixation cases under two weight bearing
124 conditions (Fig. 1).

125 **2.1 Experimental methodology**

126 In a parallel experimental study [21], five PFF fixation models using large left synthetic
127 femurs (fourth generation composite femur, Sawbones Worldwide, WA, USA) were tested
128 and the one with the average stiffness was selected for this study (average specimen). In
129 brief, the femoral condyle (distal 60mm of the femur) was removed and a total hip
130 arthroplasty was performed using an Exeter femoral stem (V40;size N°0;offset 37.5) and head
131 (28mm diameter - Stryker, NJ, USA) both made of SS. The stem was inserted into the
132 femoral canal and cemented using polymethylmethacrylate (PMMA) cement (Simplex P,
133 Stryker, NJ, USA). A transverse fracture was created 10mm below the tip of the stem and
134 completely reduced with an eight hole SS locking plate (length: 155mm; width: 17.5mm;
135 thickness: 5mm) where there was ca. 1mm of gap at the plate-bone interface. Unicortical
136 screws (outer diameter: 5mm; length: 13mm) and bicortical screws (outer diameter: 5mm;
137 Length: 40mm - Stryker, NJ, USA) were used in the three most proximal and distal holes of
138 the plate respectively, leaving two empty screw holes across the fracture site. The specimen
139 was also taken to Leeds General Infirmary (Leeds, UK) where an antero-posterior x-ray
140 (Multix Fusion, Siemens, Erlangen, Germany) was taken to evaluate the construct.

141 The specimen was instrumented with eight uniaxial strain gauges (Tokyo Sokki
142 Kenkyujo, Tokyo, Japan) located on the medial side of the femur 0, 40, 80 and 200mm below
143 the lesser trochanter (SG1-SG4), on the lateral side of the femur 200mm below the lesser
144 trochanter (SG5), and on the lateral side of the plate below the third (SG6), fourth (SG7) and
145 fifth (SG8) most proximal screw holes (see Fig. 2). The distal end of the specimen was fully
146 fixed using PMMA cement and grub screws (i.e. non-surgical headless screws used here
147 purely for mechanical purposes) into a cylindrical housing and mounted on a materials testing
148 machine (Instron, MA, USA) at 10° adduction in the frontal plane and aligned vertically in
149 the sagittal plane. This position simulates anatomical one-legged stance [22]. An axial load of

150 500N, corresponding to recommended partial weight bearing following stable plate fixation
151 [23] was applied to the femoral head stem via a hemispherical cup.

152 The stiffness was calculated based on the slope of the load-displacement data obtained
153 from the material testing machine. The strain was measured in all the strain gauges at the
154 maximum load. The fracture movement was recorded using two digital cameras (Canon,
155 Tokyo, Japan) placed on the medial and lateral side of the femur, by photographing before
156 loading and at 500N. Movements of two markers on each side on the proximal and distal
157 bony fragments were then digitized using a custom written program in MATLAB
158 (MathWorks, MA, USA). Following testing, an unstable fracture was simulated by cutting the
159 bone 5mm above and below the existing fracture line to increase the fracture gap to 10mm.
160 The specimen was then reloaded to 500N and the measurements repeated.

161 **2.2 Computational methodology**

162 **Model development:** A computer aided design (CAD) model of the synthetic femur was
163 obtained from Biomed Town through the BEL repository managed by the Intituti Ortopedici
164 Rizzoli (Bologna, Italy) [24]. The model consisted of three segments: the cortical bone and
165 the proximal and distal cancellous bone. CAD files of the stem and locking plate were
166 provided by manufacturer (Stryker, NJ, USA). The model was assembled in SolidWorks
167 (Dassault Systemes, MA, USA). First, virtual total hip arthroplasty was performed where the
168 stem position was determined based on AP and ML radiographs. The cement mantle was
169 reconstructed based on the CT images of a reamed specimen. Second, a transverse fracture
170 was created by dividing the construct into two halves that were fixed using the same screw
171 and plate configuration as the experimental model ('stable model'- Fig. 2). Lastly, a separate
172 model was developed in which a fracture gap of 10mm was induced similar to the
173 experimental procedure ('unstable model'). In both models, the distal PMMA cement, screws
174 and cylindrical pot that were used in the experimental model to fix the specimen were also

175 modelled to include the effect of deformation in this region. The models were then exported
176 to a finite element package (ABAQUS v. 6.9, Dassault Systemes, MA, USA) for analysis.

177 **Material properties:** All sections were assigned isotropic material properties with an elastic
178 modulus of 16.3GPa for cortical bone [25], 0.15GPa for cancellous bone [18], 2.45GPa for
179 cement [18], 200GPa for SS [17] and 110GPa for Ti [17]. A Poisson's ratio of 0.3 was used
180 for all materials [17].

181 **Interactions:** The interfaces at the cancellous to cortical bone, cement to bone, grub screws to
182 cement, and screw head to plate were fixed. Contact conditions were specified with hard
183 normal contact stiffness. A coefficient of friction of 0.3 was used at the stem to cement,
184 housing to cement, plate to bone and bone to bone (i.e. fracture site in the stable model)
185 interfaces [26-29]. Screw-bone interfaces were modelled using an approach described
186 elsewhere [30], which was shown to lead to closer agreement between experimental and
187 computational models when modelling screw-bone fixation. In brief, sliding contact
188 conditions were created at the screw-bone interface, while screw pull-out/push-in was resisted
189 by attaching two spring elements between the screw end and medial side of the bone along the
190 screw shaft. A frictionless contact with normal contact stiffness of 600N/mm was used [31].
191 The total spring stiffness of bicortical screws was 3141N/mm that was halved for the
192 unicortical screws [32], corresponding to reported screw pull-out data.

193 **Boundary conditions and loads:** The constructs were loaded to replicate the experimental set
194 up. The distal cylindrical pot was fixed in all directions while the stem femoral head was
195 loaded under axial load of 500N.

196 **Mesh sensitivity:** Tetrahedral (C3D10M) elements were used to mesh all of the components
197 in ABAQUS. Convergence was tested by increasing the number of elements from 70,000 to
198 1,600,000 in five steps. The solution converged on the parameter of the interest ($\leq 5\%$ - axial
199 stiffness, strain, stress and fracture movement) with over one million elements.

200 **Measurements:** In all models, axial stiffness was calculated by dividing the magnitude of
201 axial load by the displacement of the proximal section of the specimen. Strain was averaged
202 from four nodes corresponding to the strain gauge attachment sites in the experimental model.
203 Fracture movement was quantified from the displacement coordinates of the nodes
204 corresponding to the position of the markers in the experiment.

205 **Simulation and analysis:** The outputs of the stable and unstable fracture models were first
206 compared to the experimental results. In the case of the strain measurements, the agreement
207 was measured using the concordance correlation coefficient (CCC) [33]. The properties of the
208 plates and screws in both models were then changed to Ti and the models reanalysed. To test
209 the performance of the PFF fixations under higher loadings that can occur during full weight
210 bearing, all the models were also analysed under axial loading of 2300N [22].

211

212 **3. Results**

213 A comparison between the experimental and computational models in terms of axial stiffness,
214 surface strain measurement and fracture movement showed that:

215 (1) The computational models overestimated the axial stiffness of the stable and unstable
216 PFF fixation construct by 121% and 61% respectively. However, computational
217 models predicted 78% reduction in the stiffness of the stable compared to the unstable
218 PFF fixation which is comparable to 70% reduction that was shown by the
219 experimental model (Fig. 3).

220 (2) There was a high level of agreement in the strain measurements between the
221 experimental and computational models with a CCC of 0.77 for the stable and 0.8 for
222 unstable construct cases (Fig. 4).

223 (3) The computational models underestimated the axial fracture movement. However,
224 both models in the case of stable PFF fixation showed less than 0.1mm movement

225 whereas in the case of unstable PFF fixation, the movement was in the range of 0.2 to
226 0.7mm. Also both models showed unparallel axial fracture movement between the
227 near and far cortex in both stable and unstable PFF fixation.

228 The computational predicted strain values, maximum von Mises stress on the plate, and
229 fracture movement for models with the different plate properties under the two axial loading
230 cases are presented in Tables 1 and 2. The results showed that:

231 (1) Strain on the proximal section of the femur (SG1-SG3) was lower in the unstable
232 compared to the stable PFF fixation; nevertheless the strain magnitudes were similar
233 in both cases under the two loading cases and with the two plate materials. The strain
234 in the distal section of the bone was higher in the unstable compared to the stable
235 fixation.

236 (2) Strain and stress on the plate were considerably higher in the unstable compared to the
237 stable fixation. For example, the maximum von Mises stress on the SS plate under
238 500N loading in unstable PFF fixation was ca. 32 times higher than the stable fixation.
239 Increasing the axial loading from 500N to 2300N led to ca. 4.6 times greater
240 maximum von Mises stress on the plate with similar conditions. Further, altering the
241 plate property from SS to Ti led to ca. a 1.3 and 1.1 fold reduction in the maximum
242 von Mises stress on the plate under same loading for stable and unstable PFF fixation
243 respectively.

244 (3) Fracture movement in the stable PFF fixation was less than 0.1mm in all cases,
245 whereas in the unstable fixation at 500N it was within the range of 0.2-1mm, and at
246 2300N it was above 1mm for both SS and Ti plate in the medial view. Fracture
247 movement in the medial view was higher than the anterior view.

248 Maximum von Mises stress in the stable PFF fixation was on the lateral side of the plate
249 across the empty screw hole in all cases, whereas in the unstable fixation it was on the medial

250 side of the plate between the third and fourth screw hole (Fig. 6). In the unstable PFF fixation
251 under 2300N load, the titanium plate came into contact across the empty screw hole with the
252 proximal bony fragment this led to a concentration of stress on the plate, however such
253 contact did not occur under same loading condition in the SS plate (Fig. 6).

254

255 **4. Discussion**

256 Quantifying the effect of fracture stability and loading on the relative risk of plate fracture for
257 PFF fixations does not appear to have been undertaken previously. In this study an FE model
258 was described and used to quantify the effect of aforementioned parameters in SS and Ti
259 locking plate fixation. In each case, peak stress values were compared with the yield stress
260 and fatigue life (as a result of cyclic loading) for each material, an indication of plate fracture
261 risk.

262 The FE model was first compared with experimental tests. A strong correlation was
263 found between the strain predictions of the experimental and computational models.
264 However, the computational models overestimated the stiffness of the experimental models.
265 This could be due to a number of factors, such as over-estimation of material or interaction
266 properties. FE models have been shown to be sensitive to the choice of interaction properties
267 at the interfaces [26,28,29]. The fact that there was a closer agreement between the
268 computational and experimental models of the unstable fracture (i.e. without interaction at
269 fracture site) compared to the stable fracture (i.e. with interactions at fracture site - Fig. 4)
270 indicates that this was one source of error. Despite this overestimation, it was reassuring that
271 both experimental and computational model captured very similar percentage of reduction in
272 the stiffness of stable compare to unstable PFF fixation (ca. 70% vs. 78% respectively). This,
273 coupled with the good agreement in strain within the area of interest in the fixation plate,

274 provided confidence that the FE model was suitable for making the comparisons between
275 different fixation scenarios required for this study.

276 The overestimation of the stiffness clearly explains the underestimation of the fracture
277 movement predicted by the FE models. Nevertheless, the movement in both experimental and
278 FE models in the stable PFF fixation was below the threshold that is suggested to promote
279 callus formation (0.2-1mm) [13,14,34]. This rigid fixation explains why callus did not form in
280 some of the previous case reports of rigid PFF fixations [5,19]. Rigid PFF fixation can be
281 avoided by increasing the bridging length [35] or using alternative screw designs such as far
282 cortical locking screws [36].

283 As anticipated, the load sharing between the plate and the bone in the case of the stable
284 fracture caused higher compressive strain in the proximal bone and reduced tensile strain on
285 the surface of the plate (Table 1), when compared to the unstable fracture cases. Where this
286 load sharing existed, the maximum stress concentrations on the plate did not exceed the
287 fatigue limit (Table 3), even for the equivalent of five years of normal walking [17]. For the
288 unstable fracture cases, where the plate was the sole loading bearing component, maximum
289 plate stress was much higher. In the case of partial weight bearing was within the fatigue limit
290 of the SS and Ti commonly used to manufacture implants (see Table 3). Furthermore, the
291 fracture movement was within the range of 0.2-1mm [13,14,34]. However, under the higher
292 load of 2300N, not only was the fracture movement above the aforementioned range but also
293 the von Mises stress reached the yield level of both SS and Ti (Table 3) [17,37], suggesting
294 that mechanical damage could occur to the plate within a relative small number of cycles.

295 These findings have two clinical consequences. First, unstable fractures could be
296 potentially treated with a single 5mm thick SS locking plate using the screw configuration
297 applied in this study provided that patient is restricted to partial weight bearing. Second, in the
298 cases where complete fracture reduction has not been achieved and a fracture gap is present

299 postoperatively, the patient should be warned that full weight bearing can potentially lead to
300 mechanical failure of the fixation [38]. Nevertheless, orthopedic trauma surgeons may
301 consider long stem revision and bypassing the fracture gap or biological fixation in addition to
302 locking plates in the case of unstable PFF fractures, particularly in active patients [5,8,39].

303 Results here highlight that fracture stability and postoperative weight bearing can have a
304 more pronounced effect on the performance of plate fixation than the material properties of
305 the fixation, given that other biomechanical factors such as bridging length are the same
306 nevertheless patient variability cannot be ignored [40]. Lujan et al [41] suggested that Ti
307 plates can enhance callus formation when compared to the SS plate in distal femoral fractures.
308 The present study provides some quantification of the increase in plate bending and fracture
309 movement for Ti, which may contribute to enhanced callus formation. However, the yield
310 stress and fatigue limit of Ti are lower than that of SS (Table 3). Therefore the risk of failure
311 remains unless early callus formation and the resulting load sharing with the bone can be
312 created through careful postoperative loading.

313 A noteworthy, unanticipated result occurred in the unstable PFF fixation under axial
314 load of 2300N, the Ti plate came into contact across the fracture site to the proximal bony
315 fragment (see dotted rectangles in Fig. 6). FE models in this study predicted stress riser effect
316 on the plate fixation as a result of this contact. However, care must be taken in the
317 interpretation of this result since FE models in this study: (1) did not include any failure
318 criteria for the bone or other segments (2) considered a static loading where in reality the
319 fixation construct is under cyclic loading where it is likely that a small bony fragment at the
320 plate-bone contact zone will fail earlier than the plate. Nonetheless, this finding highlights the
321 importance of plate-bone gap particularly in Ti locking plate fixation. Such a gap has been
322 suggested to increase the flexibility of the fixation [42], prevent necrosis and ensure blood
323 supply to the fracture site that plays a crucial role in fracture healing process [43].

324 In conclusion, in the case of unstable fractures or where a fracture gap is present post
325 operatively, it is possible for a single locking plate fixation to provide the required mechanical
326 environment for callus formation without significant risk of plate fracture, provided partial
327 weight bearing is followed. Full weight bearing significantly increases the risk of plate
328 fracture regardless of the whether SS or Ti plates are used. In cases where partial weight
329 bearing is unlikely, additional biological fixation could be considered. The FE model
330 described in this study will be used in future studies to investigate alternative fixation
331 methods for PFF fixation.

332

333

334

335

336

337

338

339

340

341

342

343

344

345

346

347

348

349 **References**

- 350 1. Duncan CP, Masri BA. Fractures of the femur after hip replacement. Instr Course Lect
351 1995; 44:293.
- 352 2. Parvizi J, Rapuri VR, Purtill JJ, *et al.* Treatment protocol for proximal femoral
353 periprosthetic fractures. J Bone Joint Surg [Am] 2004; 86:8.
- 354 3. Lindahl H, Malchau H, Oden A, *et al.* Risk factors for failure after treatment of a
355 periprosthetic fracture of the femur. J. Bone Joint Surg [Br] 2006; 88:26.
- 356 4. Tsiridis E, Narvani AA, Timperley JA, *et al.* Dynamic compression plates for Vancouver
357 type B periprosthetic femoral fractures: a 3-year follow-up of 18 cases. Acta Orthop 2005;
358 76:531.
- 359 5. Buttaro MA, Farfalli G, Paredes Nunez M, *et al.* Locking compression plate fixation of
360 Vancouver type-B1 periprosthetic femoral fractures. J Bone Joint Surg [Am] 2007;
361 89:1964.
- 362 6. Mont MA, Maar DC, Fractures of the ipsilateral femur after hip arthroplasty. A statistical
363 analysis of outcome based on 487 patients. J Arthroplasty 1994; 9:511.
- 364 7. Graham SM, Moazen M, Leonidou A, *et al.* Locking plate fixation for Vancouver B1
365 periprosthetic femoral fractures: a critical analysis of 135 cases. J Orthop Sci (in press).
- 366 8. Talbot M, Zdero R, Schemitsch EH, Cyclic loading of periprosthetic fracture fixation
367 constructs. J Trauma 2008; 64:1308.
- 368 9. Dennis MG, Simon JA, Kummer FJ, *et al.* Fixation of periprosthetic femoral shaft
369 fractures occurring at the tip of the stem: a biomechanical study of 5 techniques. J
370 Arthroplasty 2000; 15:523.
- 371 10. Peters CL, Bachus KN, Davitt JS, Fixation of periprosthetic femur fractures: a
372 biomechanical analysis comparing cortical strut allograft plates and conventional metal
373 plates. Orthopedics 2003; 26:695.

- 374 11. Zdero R, Walker R, Waddell JP, *et al.* Biomechanical evaluation of periprosthetic femoral
375 fracture fixation. *J Bone Joint Surg [Am]* 2008; 90:1068.
- 376 12. Moazen M, Jones AC, Jin Z, *et al.* Periprosthetic fracture fixation of the femur following
377 total hip arthroplasty: a review of biomechanical testing. *Clin Biomech* 2011; 26:13.
- 378 13. Goodship AE, Kenwright J. The influence of induced micromovement upon the healing of
379 experimental tibial fractures. *J Bone Joint Surg [Br]* 1985; 67:250.
- 380 14. Claes L, Wilke H-J, Augat P, *et al.* Effect of dynamization of gap healing of diaphyseal
381 fractures under external fixation. *Clin Biomech* 1995; 8:227.
- 382 15. Oh JK, Sahu D, Ahn YH, *et al.* Effect of fracture gap on stability of compression plate
383 fixation: a finite element study. *J Orthop Res* 2010; 28:462.
- 384 16. Mihalko WM, Beaudoin AJ, Cardea JA, *et al.* Finite-element modelling of femoral shaft
385 fracture fixation techniques post total hip arthroplasty. *J Biomech* 1992; 25:469.
- 386 17. Chen G, Schmutz B, Wullschlegler M, *et al.* Computational investigation of mechanical
387 failures of internal plate fixation. *Proc Inst Mech Eng Part H* 2010; 224:119.
- 388 18. Shah S, Kim SYR, Dubov A, *et al.* The biomechanics of plate fixation of periprosthetic
389 femoral fractures near the tip of a total hip implant: cables, screws, or both? *Proc Inst*
390 *Mech Eng Part H* 2011; 225:845.
- 391 19. Moazen M, Jones AC, Leonidou A, *et al.* Rigid versus flexible plate fixation for
392 periprosthetic femoral fracture - computer modelling of a clinical case. *Med Eng Phys*
393 2012; 34:1041.
- 394 20. Anderson AE, Ellis BJ, Weiss JA. Verification, validation, and sensitivity studies in
395 computational biomechanics. *Comp Meth Biomech Biomed Eng* 2007; 10:171.
- 396 21. Mak JH, Etchels LW, Moazen M, *et al.* Locking plates versus long stem fixation to
397 restore pre-fracture mechanics of a B1 periprosthetic femoral fracture. *Proceedings of the*
398 *2012 Annual Meeting of Orthopaedic Research Society. San Francisco. USA.*

- 399 22. Bergmann G, Deuretzbacher G, Heller M, *et al.* Hip contact forces and gait patterns from
400 routine activities. *J Biomech* 2001; 34:859.
- 401 23. Ryf CR, Arraf J: Postoperative fracture treatment: general considerations. p. 447. In Ruedi
402 TP, Buckley RE, Moran CG, eds. *AO principles of fracture management*, 2ed. Davos: AO
403 Publishing; 2007.
- 404 24. Desmarais-Trépanier C. “femur_sawbone.zip, From the Biomechanics European
405 Laboratory _BEL_, Finite Element Mesh Repository,” <http://www.tecno.ior.it/VRLAB>.
406 2009.
- 407 25. Heiner AD. Structural properties of fourth-generation composite femurs and tibias. *J*
408 *Biomech* 2008; 41:3282.
- 409 26. Hayes WC, Perren SM. Plate-bone friction in the compression fixation of fractures. *Clin*
410 *Orthop* 1972; 89:236.
- 411 27. Shockey JS, Von Fraunhofer JA, Seligson D. A measurement of the coefficient of static
412 friction of human long bones. *Surf Technol* 1985; 25:167.
- 413 28. Mann KA, Bartel DL, Wright TM, *et al.* Coulomb frictional interfaces in modeling
414 cemented total hip replacements: a more realistic model. *J Biomech* 1995; 28:1067.
- 415 29. Nuno N, Groppetti R, Senin N. Static coefficient of friction between stainless steel and
416 PMMA used in cemented hip and knee implants. *Clin Biomech* 2006; 21:956.
- 417 30. Moazen M, Mak JH, Jones AC, *et al.* Evaluation of a new approach for modelling the
418 screw-bone interface in a locking plate fixation – a corroboration study. *Proc Inst Mech*
419 *Eng Part H*.
- 420 31. Bernakiewicz M, Viceconti M. The role of parameter identification in finite element
421 contact analysis with reference to orthopaedic biomechanics applications. *J Biomech*
422 2002; 35:61.

- 423 32. Zdero R, Rose S, Schemitsch EH, *et al.* Cortical screw pullout strength and effective shear
424 stress in synthetic third generation composite femurs. *J Biomech Eng* 2007; 129:289.
- 425 33. Lin LI. A concordance correlation coefficient to evaluate reproducibility. *Biometrics*
426 1989; 45:255.
- 427 34. Egol KA, Kubiak EN, Fulkerson E, *et al.* Biomechanics of locked plates and screws. *J*
428 *Orthop Trauma* 2004; 18:488.
- 429 35. Stoffel K, Dieter U, Stachowiak G, *et al.* Biomechanical testing of the LCP- how can
430 stability in locked internal fixators be controlled? *Injury* 2003; 34:S-B11.
- 431 36. Bottlang M, Doornink J, Fitzpatrick DC, *et al.* Far cortical locking can reduce stiffness of
432 locked plating constructs while retaining construct strength. *J Bone Joint Surg [Am]* 2009;
433 91:1985.
- 434 37. Brunski JB: Metals In: Classes of materials used in medicine. p. 137. In Ratner BD,
435 Hoffman AS, Schoen FJ, *et al.*, eds. *Biomaterials Science: an introduction to material in*
436 *medicine*, 2ed. California: Elsevier Academic Press; 2004.
- 437 38. Augat P, Merk J, Ignatius A, *et al.* Early, full weight bearing with flexible fixation delays
438 fracture healing. *Clin Orthop Relat Res* 1996; 328:194.
- 439 39. Haddad FS, Duncan CP, Berry DJ, *et al.* Periprosthetic femoral fractures around well-
440 fixed implants: use of cortical onlay allografts with or without a plate. *J Bone Joint Surg*
441 *[Am]* 2002; 84:945.
- 442 40. Henderson CE, Bottlang M, Marsh JL, *et al.* Does locked plating of periprosthetic
443 supracondylar femur fractures promote bone healing by callus formation? Two cases with
444 opposite outcomes. *Iowa Orthop J* 2008; 28:73.
- 445 41. Lujan TL, Henderson CE, Madey SM, *et al.* Locked plating of distal femur fracture leads
446 to inconsistent and asymmetric callus formation. *J Orthop Trauma* 2010; 24:156.

447 42. Ahmad M, Nanda R, Bajwa AS, *et al.* Biomechanical testing of the locking compression
448 plate: when does the distance between bone and implant significantly reduce construct
449 stability? *Injury* 2007; 38:358.

450 43. Perren SM. Evolution of the internal fixation of long bone fractures. The scientific basis
451 of biological internal fixation: choosing a new balance between stability and biology. *J*
452 *Bone Joint Surg [Br]* 2002; 84:1093.

453 **Acknowledgments**

454 This work is supported by British Orthopaedic Association (BOA) through the Latta
455 Fellowship and was partially funded through WELMEC (Wellcome Trust & EPSRC,
456 under grant WT 088908/Z/09/Z) and LMBRU through NIHR (National Institute for
457 Health Research). We thank Simon M Graham for his assistance during the
458 experimental work. The components for the experimental and computational models
459 were provided by Stryker (SA, Switzerland).

460

461

462

463

464

465

466

467

468

469

470

471

472 **Figure legends**

473 **Fig. 1** A schematic of this study.

474 **Fig. 2** Experimental and computational model of PFF fixation. SG1-SG8 highlight the strain
475 gauge attachment area.

476 **Fig. 3** Comparison between the experimental and computational stiffness of the stable and
477 unstable PFF fixation based on average specimen.

478 **Fig. 4** Comparison between the experimental and computational strain of the stable and
479 unstable PFF fixation based on the average specimen.

480 **Fig. 5** Comparison between the experimental and computational fracture movement on the
481 anterior (A) and medial (B) view of the stable and unstable PFF fixation based on the average
482 specimen.

483 **Fig. 6** Comparison between von Mises stress contour plot of all cases. The regions of
484 maximum von Mises stress are highlighted by ovals. Dotted rectangles highlight the plate to
485 bone contact that did not occur in the stainless steel (SS) plate and occurred in the titanium
486 (Ti) plate fixation under high axial loading of 2300N.

487

488

489

490

491

492

493

494

495

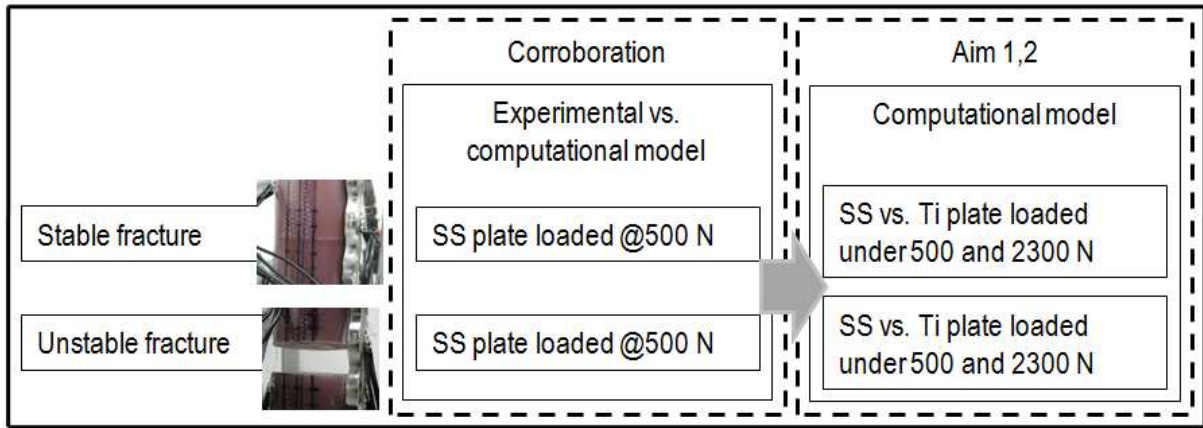
496

497 **Table legends**

498 **Table 1** Summary of the strain measurements and maximum von Mises stress on the plate.

499 **Table 2** Summary of the axial fracture movement (mm) of PFF fixation constructs.

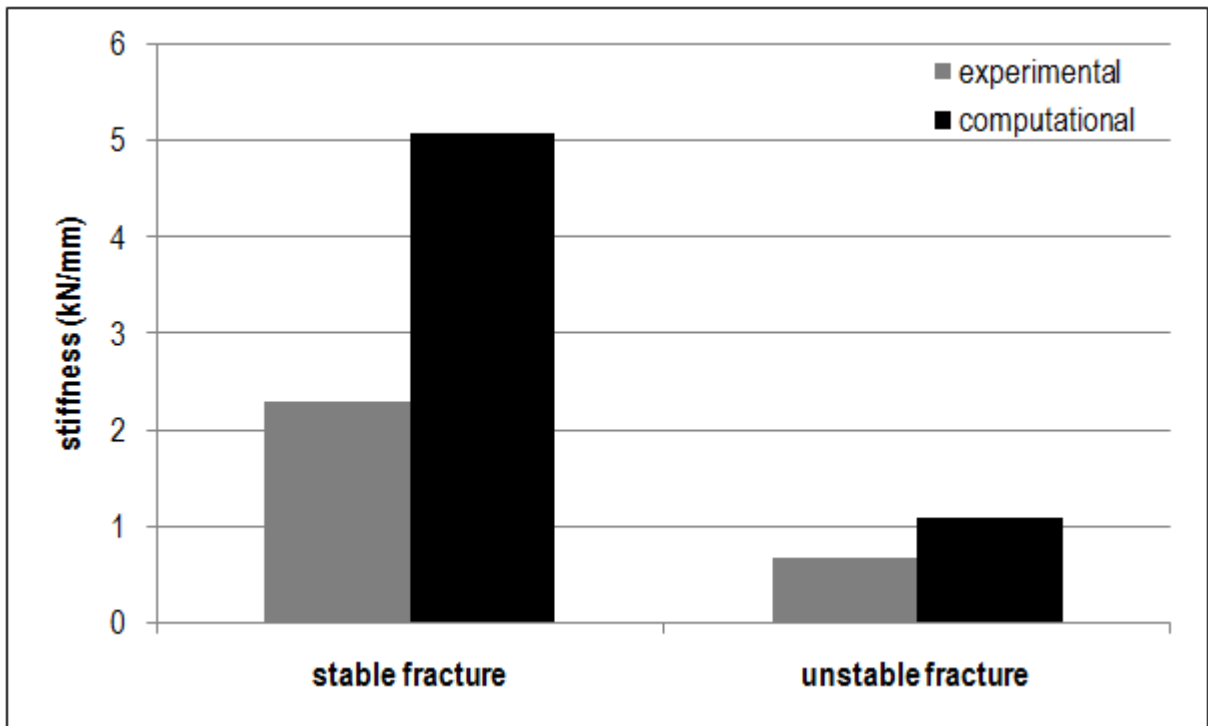
500 **Table 3** Summary of yield stress, ultimate tensile stress and fatigue limit of SS and Ti [37].



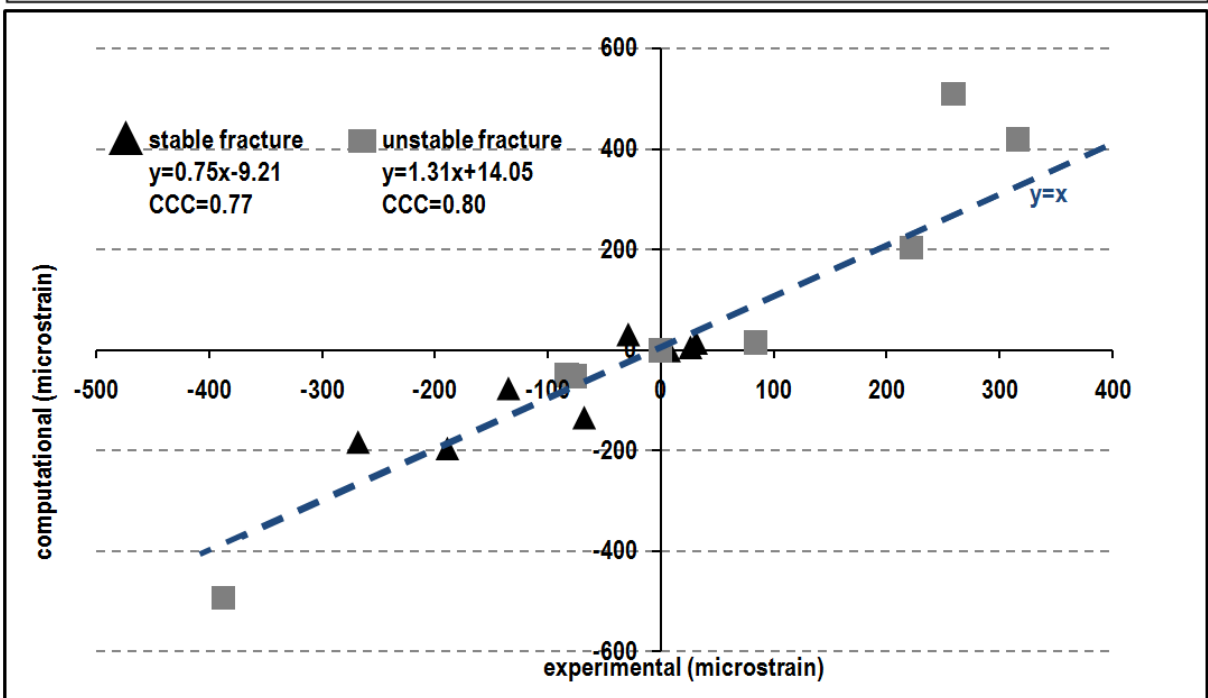
501



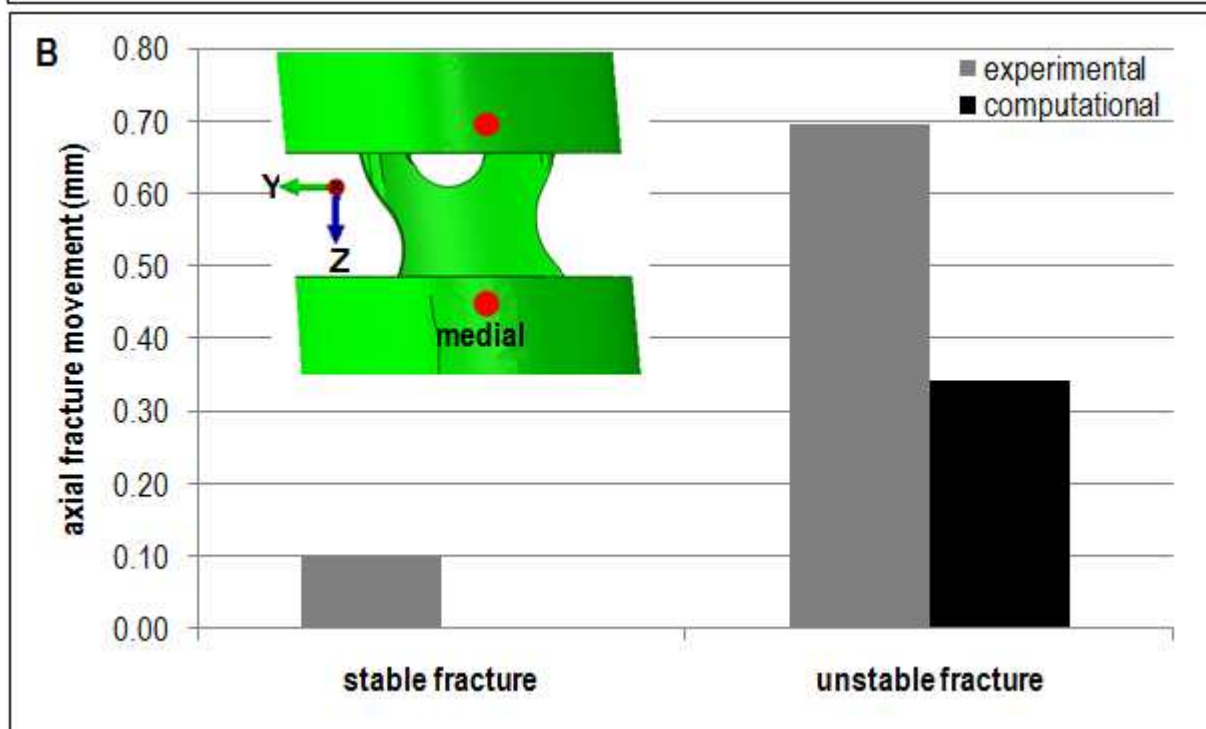
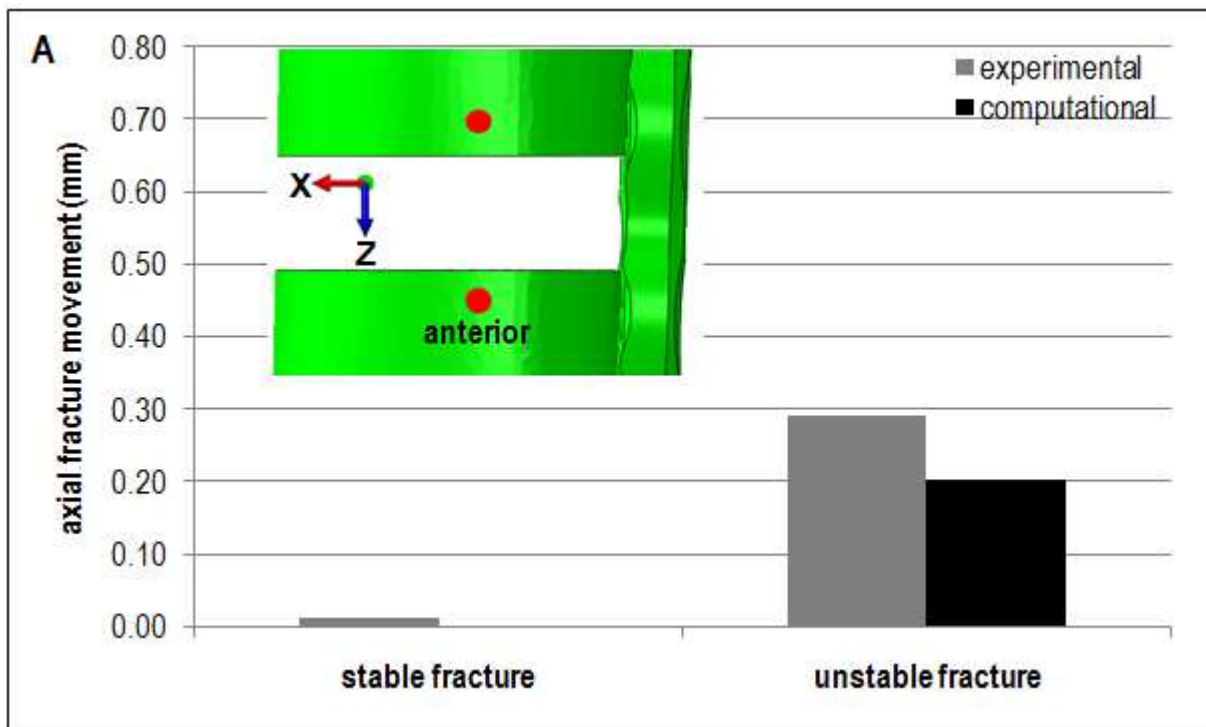
502



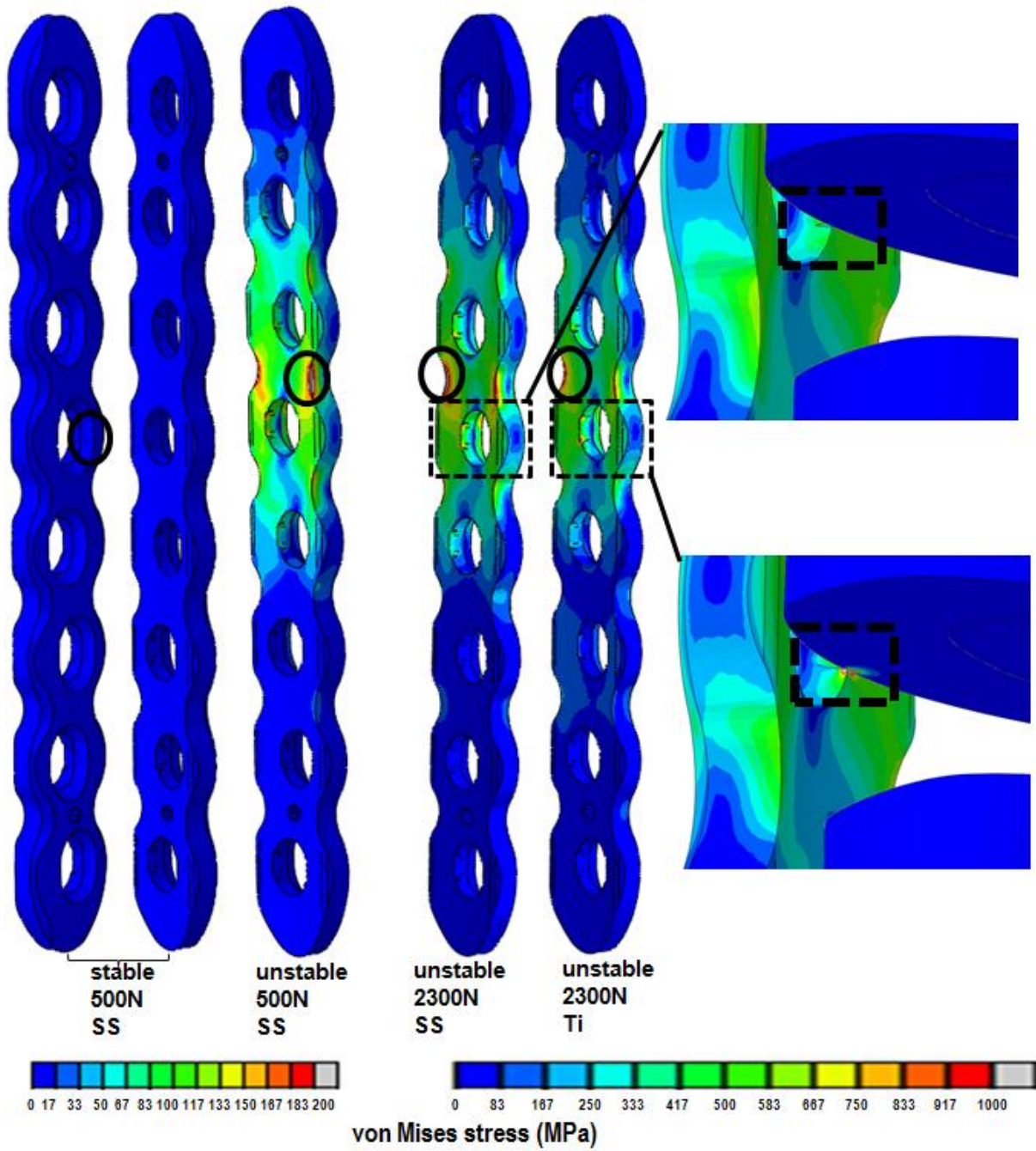
503



504



505



506

507

508

509

510

511

512

513

514 **Table 1** Summary of the strain measurements and maximum von Mises stress on the plate.

	Stable				Unstable			
Axial load (N)	500	2300	500	2300	500	2300	500	2300
Material	SS	SS	Ti	Ti	SS	SS	Ti	Ti
SG1	-76	-349	-75	-355	-50	-230	-44	-215
SG2	-196	-916	-197	-918	-52	-260	-44	-263
SG3	-183	-808	-186	-824	-1	-5	-1	-6
SG4	32	157	33	161	419	2059	446	2182
SG5	-134	-624	-135	-628	-493	-2392	-519	-2506
SG6	15	61	20	84	509	2510	816	3813
SG7	6	23	7	28	204	985	274	1447
SG8	0	2	0	0	15	41	-43	-192
Maximum von Mises stress on the plate (MPa)	8	35	6	28	255	1258	227	1084

515

516

517 **Table 2** Summary of the axial fracture movement (mm) of PFF fixation constructs.

	Stable				Unstable			
Axial load (N)	500	2300	500	2300	500	2300	500	2300
Material	SS	SS	Ti	Ti	SS	SS	Ti	Ti
Anterior	0.001	0.007	0.001	0.007	0.202	0.973	0.249	1.197
Medial	0.003	0.016	0.003	0.016	0.343	1.665	0.413	1.976

518

519 **Table 3** Summary of yield stress, ultimate tensile stress and fatigue limit of SS and Ti [37].

Material	SS	Ti
ASTM designation	F138, F139	F67
Condition	30% Cold worked	30% Cold worked
Ultimate tensile stress (MPa)	930	760
Yield stress (MPa)	792	485
Fatigue limit (at 10⁷ cycles-MPa)	310-448	300

520

521

522